ISSN 0036-0236, Russian Journal of Inorganic Chemistry, 2018, Vol. 63, No. 1, pp. 1–15. © Pleiades Publishing, Ltd., 2018.
Original Russian Text © E.P. Simonenko, N.P. Simonenko, E.K. Papynov, E.A. Gridasova, V.G. Sevastyanov, N.T. Kuznetsov, 2018, published in Zhurnal Neorganicheskoi Khimii, 2018, Vol. 63, No. 1, pp. 3–18.

SYNTHESIS AND PROPERTIES OF INORGANIC COMPOUNDS

Production of HfB_2–SiC (10–65 vol % SiC) Ultra-High-Temperature Ceramics by Hot Pressing of HfB_2–(SiO_2–C) Composite Powder Synthesized by the Sol–Gel Method

E. P. Simonenko[a, *], N. P. Simonenko[a], E. K. Papynov[b, c], E. A. Gridasova[c], V. G. Sevastyanov[a], and N. T. Kuznetsov[a]

[a] *Kurnakov Institute of General and Inorganic Chemistry, Russian Academy of Sciences, Moscow, 119991 Russia*
[b] *Institute of Chemistry, Far-Eastern Branch, Russian Academy of Sciences, Vladivostok, 690022 Russia*
[c] *Far-Eastern Federal University, Vladivostok, 690950 Russia*
**e-mail: ep_simonenko@mail.ru*

Received September 4, 2017

Abstract—The formation of HfB_2–SiC (10–65 vol % SiC) ultra-high-temperature ceramics by hot pressing of HfB_2–(SiO_2–C) composite powder synthesized by the sol–gel method was studied. By the example of HfB_2–30 vol % SiC ceramic, it was shown that the synthesis of nanocrystalline silicon carbide is completed at temperatures of as low as ≥1700°C (crystallite size 35–39 nm). The production of the composite materials with various contents of fine silicon carbide at 1800°C demonstrated that the samples of the composition HfB_2–SiC (20–30 vol % SiC) are characterized by the formation of SiC crystallites of the minimum sizes (36–38 nm), by the highest density (89%), and by higher oxidation resistance during heating in an air flow to 1400°C.

DOI: 10.1134/S0036023618010187

Ceramics based on zirconium or hafnium diboride and modified by silicon carbide offer great opportunities for designing aircraft components and engine parts serviceable during aerodynamic heating in an oxygen-containing gas flow [1–32]. In this context, much attention is given both to looking for methods for improving the mechanical properties of the materials, particularly their thermal cycling strength, to studying the high-temperature oxidation mechanism at various oxygen contents and different pressures, and to developing methods for increasing oxidation resistance.

At the present time, there is a consensus that, for increasing the oxidation resistance (as well as for reaching the optimum mechanical properties) of HfB_2(ZrB_2)–SiC ultra-high-temperature ceramics (UHTCs), one should strive for the maximally uniform distribution of the components in each other and the minimum grain size [33–40]. For this purpose, the mildest temperature conditions of UHTCs production were sought, methods for introducing additives that inhibit the significant growth of HfB_2(ZrB_2) grains were developed, and nanosized components were proposed to be used.

In our opinion, chemical modification of the surface of HfB_2 powder with nanosized oxidation-reactive silicon carbide by the sol–gel method (Fig. 1) will improve the uniformity of the mutual distribution of the components in the ceramic and can influence its oxidation mechanism.

The oxidation of HfB_2(ZrB_2)–SiC composite ceramics usually begins with the boride component, and the formed B_2O_3 intensely evaporates, freeing the surface of the unoxidized material and favoring the further interaction of HfB_2 with oxygen. This process slows down only after the second component (SiC) begins (at higher temperatures) to be oxidized due to the formation of more viscous borosilicate glass. If the surface of HfB_2 particles is coated with a layer of nanocrystalline silicon carbide, which is much more reactive than a coarse powder (fine powders begin to be oxidized at temperatures of as low as ~700–1000°C, depending on the particle size [40–44]), then borosilicate glass preventing rapid oxidation should form at lower temperatures. Moreover, the SiC layer creates additional diffusion limitations to the interaction of oxygen with HfB_2 particles.

In this connection, in recent years, a diversity of methods for producing HfB_2(ZrB_2)–SiC composite powders have been developed [44–61], among which, from the standpoint of the possibility of the moderate-temperature synthesis of the finest products with a uniform mutual distribution of the components, the sol–gel method seems to be the most promising [44–51]. Previously [44], we synthesized HfB_2–SiC (10–

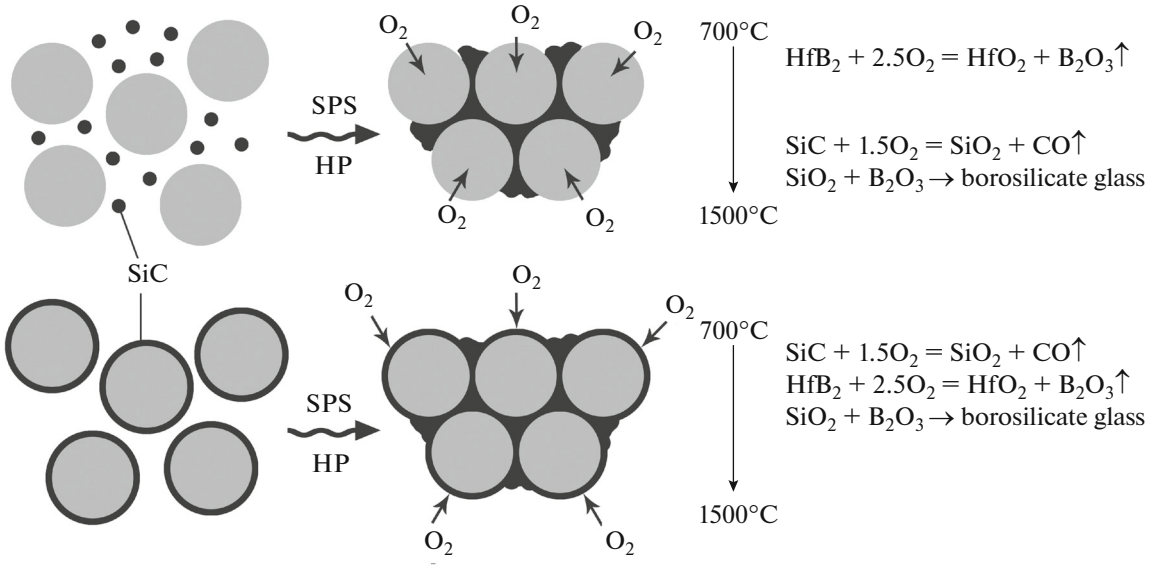

Fig. 1. Scheme of the oxidation of HfB_2–SiC UHTCs based on individual powders HfB_2 and SiC and on composite powders HfB_2–SiC. SPS, spark plasma sintering; HP, hot pressing.

65 vol % SiC) composite powder by chemical modification of microdispersed HfB_2 powder with nanocrystalline silicon carbide obtained by tetraethoxysilane hydrolysis in the presence of phenol–formaldehyde resin with subsequent gel formation, carbonization at 400°C at reduced pressure, and carbothermal synthesis at 1400°C for 4 h in a dynamic vacuum. It was noted that the sample containing 30 vol % SiC experienced the minimum weight gain due to the oxidation of the components. In reviews [45, 46], the sol–gel method was indicated to be advantageous for producing nonoxide ceramic powders, including zirconium and hafnium diborides and MB_2–SiC(–MC) composite powders, where M = Zr, Hf. Wang et al. [47] obtained ZrB_2–20 vol % SiC composite powder by mixing an acetic acid solution of boric acid and sucrose with a methanol solution of zirconium isopropoxide, acetylacetone, and tetraethoxysilane with subsequent heating at 65°C for 8 h to form a gel, which after drying was stepwise heated in an argon atmosphere to 800, 1200, and 1550°C to produce globular particles ~800 nm in diameter. Cao et al. [48] performed the microwave boro/carbothermal reduction of composites obtained by mixing a distilled water solution of boric acid and glucose with an aqueous solution of zirconium oxide dichloride, glucose, and ethylene glycol and with a hydrochloric acid-acidified aqueous ethanol solution of tetraethoxysilane with subsequent heating at 80°C, drying of the formed gel, and heat treatment in an argon flow in a microwave oven. It was shown that, in this case, the desired phases ZrB_2 and SiC form at a temperature of as low as 1300°C, which is approximately 200°C lower than the temperature at which they form without microwave treatment. Zhang et al. [49] used such reagents as zirconium propoxide (with acetylacetone added) and zirconium oxide nitrate, tetraethoxysilane, boric acid, and sucrose; at the initial stage, amorphous precursor ZrO_2–SiO_2 formed, which was further reduced by boron and carbon in argon during stepwise heating to 800°C and then to 1550°C. It was noted that the obtained particles with equiaxial morphology contained simultaneously ZrB_2 and SiC and had a size of ~800 nm. In Zhao's article [50], which is ideologically related to Zhang et al.'s [49], the role of acetic acid was shown, which acts as a modifier and a component enabling one to generate hydrolyzing water in the reaction with propanol. To synthesize ZrB_2–20 vol % SiC composite powder [51], $ZrOCl_2$ and H_3BO_3 were dissolved in ethanol, phenol resin was added, and a gel was produced by increasing pH by adding aqueous ammonia. Drying and heat treatment at 1500 and 1600°C gave products that contained not only ZrB_2 and SiC, but also a small amount of ZrC. By hot pressing of the obtained ZrB_2–SiC–ZrC powder at 2250°C for 2 h, ceramic samples with a density of 97.6% were manufactured.

Earlier, we proposed a method for producing nanostructured silicon carbide ceramics at relatively low temperatures by carbothermal synthesis directly during spark plasma sintering of fine SiO_2-C composite obtained by the sol–gel method [62]. We concluded that an alternative method for synthesizing MB_2–SiC UHTCs without stages of grinding and mixing of the initial powders of zirconium or hafnium diboride and silicon carbide is promising (Fig. 2). The proposed method is based on high-temperature pressing of HfB_2–(SiO_2–C) powders that are synthesized

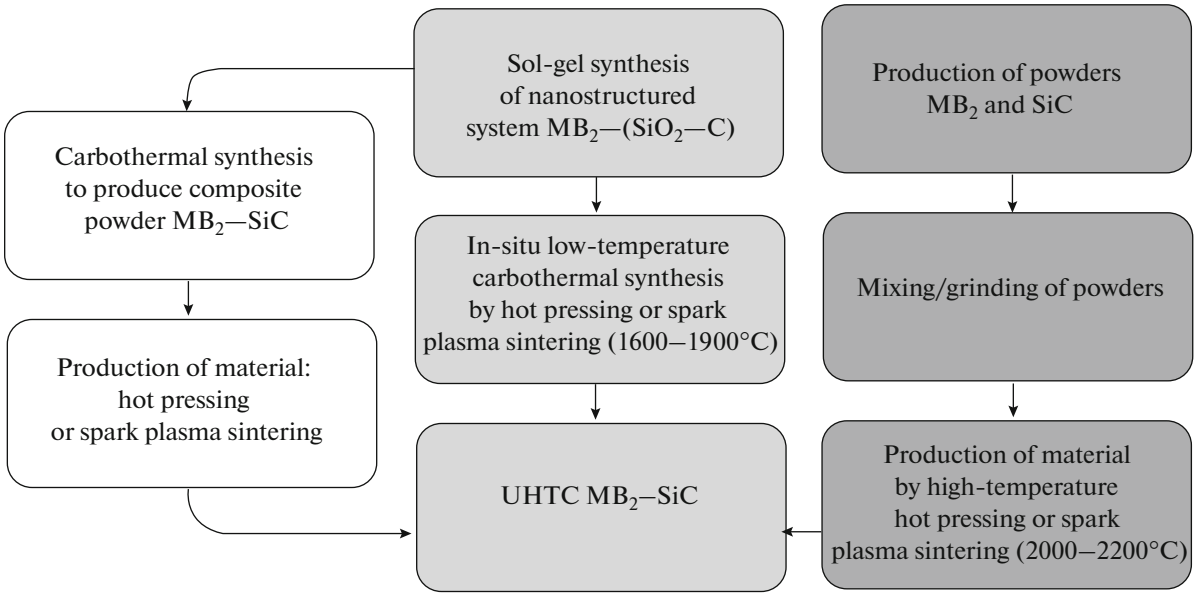

Fig. 2. Flowchart of the proposed approaches to producing MB_2–SiC (M = Zr, Hf) UHTCs (left and central columns) and the classical approach (right column).

by the sol–gel method and, hence, have elevated reactivity.

SiO_2 that is present in the initial composition plays an additional role of a sintering additive and improves compaction processes at relatively low temperatures (<2000°C) in comparison with the additive that is typically used for producing ceramics of the above composition (1900–2200°C).

Thus, the purpose of this work was to study the production of HfB_2–SiC (10–65 vol % SiC) UHTCs by hot pressing of HfB_2–(SiO_2–C) composite powders synthesized by the sol–gel method.

EXPERIMENTAL

In the experiments, we used tetraethoxysilane $Si(OC_2H_5)_4$ (special-purity grade 14-5), LBS-1 Bakelite phenol–formaldehyde varnish, formic acid CH_2O_2 (analytically pure), acetone CH_3COCH_3 (analytically pure), and hafnium diboride (pure, particle size 2–3 μm, aggregate size ~20–60 μm).

The initial HfB_2–(SiO_2–C) powder was synthesized by chemical modification of the surface of HfB_2 powder by controlled tetraethoxysilane hydrolysis in the presence of a polymer carbon source [41–44, 63] with subsequent gel formation, drying, and heat treatment of xerogels at 400°C for 2 h in a dynamic vacuum (residual pressure ~1–10 Pa).

HfB_2–SiC UHTCs were produced using a Thermal Technology HP20-3560-20 hot press. The obtained HfB_2–(SiO_2–C) powders were placed in graphite molds and rammed; the chamber was evacuated and then filled with argon, after which the pressure was brought to a desired value of 30 MPa and heating at a rate of 10 deg/min was started. To choose the temperature conditions of pressing, the compaction of HfB_2–(SiO_2–C) (30 vol % SiC equivalent) powder with subsequent carbothermal synthesis was investigated, and experiments at 1600, 1700, 1800, and 1900°C were conducted, with the heat treatment time at the maximum temperature being 15 min. As a mold release agent, a small amount of boron nitride was used.

The X-ray powder diffraction patterns of the synthesized composite powders were recorded with a Bruker D8 ADVANCE X-ray powder diffractometer within the characteristic 2θ range 34°–37° at a resolution of 0.02° at signal accumulation at a point for 2 s and within the 2θ range 5°–80° at a resolution of 0.02° at signal accumulation at a point for 0.3 s.

The IR spectra of the samples were recorded with an InfraLYuM FT-08 FTIR spectrometer using Nujol mulls between KBr plates.

Scanning electron microscopy was performed with a Carl Zeiss NVision 40 focused ion beam scanning electron microscope; the elemental composition of microregions was determined with an Oxford Instruments EDX energy-dispersive X-ray analyzer.

The compressive strength of the obtained samples of HfB_2–SiC ceramic was determined with a Shimadzu Autograph AG-X plus 50 kN precision universal/tensile tester.

The thermal behavior of the samples was studied with an SDT Q-600 combined TGA/DSC/DTA analyzer (heating rate 20 deg/min, air flow rate 250 mL/min).

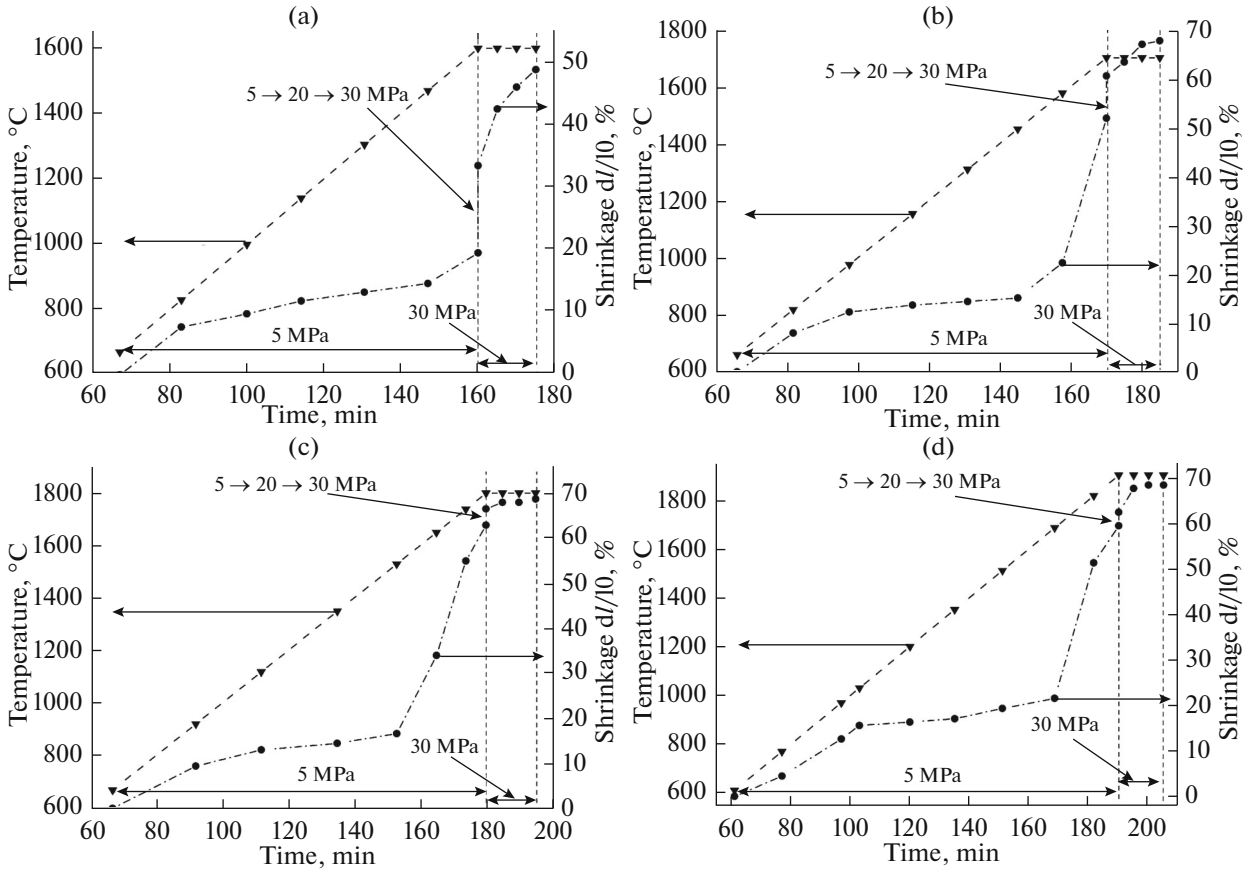

Fig. 3. Changes with time in the temperature, pressure, and corresponding shrinkage during hot pressing of HfB_2–(SiO_2–C) composite powders in the course of the production of HfB_2–30 vol % SiC UHTC: (a) 1600; (b) 1700; (c) 1800; (d) 1900°C.

RESULTS AND DISCUSSION

Production and Investigation of HfB_2–SiC (30 vol % SiC) UHTCs at Various Temperatures of Hot Pressing of HfB_2–(SiO_2–C) Composite Powder

To choose the optimum process conditions that would ensure the highest possible conversion in the carbothermal synthesis of nanocrystalline silicon carbide in HfB_2–SiC ceramics, we carried out a series of experiments involving hot pressing of HfB_2–(SiO_2–C) (30 vol % SiC calculated equivalent) powder at 1600, 1700, 1800, and 1900°C. Figure 3 presents the shrinkage curves, which are typical at the given temperatures. As one can see, even under the lowest-temperature conditions (heat treatment at 1600°C) still without applying a given pressure of 30 MPa (i.e., at a pressure of 5 MPa, the shrinkage starts to increase at a temperature of ~1500°C, which is close to the carbothermal synthesis temperature found by thermodynamic calculations under atmospheric pressure conditions [64, 65]. At temperatures ≥1600°C, the compaction process sharply accelerates. For the samples obtained by pressing at the minimum temperature 1600°C at the applied pressure 30 MPa for 15 min, there is intense compaction (~30%, definitely far from plateauing), which is likely to be due primarily to the continuing SiC synthesis and sintering involving liquid SiO_2.

At the higher sintering/synthesis temperatures (1700, 1800, and 1900°C), the shrinkage is the maximum prior to the application of the maximum pressure 30 MPa after reaching the temperature 1600°C, whereas at the final treatment stages (particularly noticeably at the maximum temperature 1900°C) the shrinkage plateaus, which may indicate the completion of the carbothermal synthesis. Statistical analysis of the shrinkage data showed (Table 1) that the average shrinkage beginning with 1700°C varies insignificantly, and dl/l_0 is the maximum at 1800°C; this is probably owing to the optimum sequence of sintering, which is favored by SiO_2 (liquid under these conditions) and the carbothermal SiC synthesis.

Figure 4 presents the appearance of typical samples obtained by hot pressing of HfB_2–(SiO_2–C) composite powder at various temperatures, some characteristics of which are given in Table 1. For all the samples obtained at the minimum process temperature (1600°C), there is a color variance between the periphery and at the center (shaded area). This is likely

Table 1. Density ρ, calculated porosity, linear shrinkage dl/l_0 during hot pressing, average crystallite size L, compressive strength σ, and weight gain Δm during heating in an air flow (under the TGA/DSC conditions to a temperature of 1400°C) for the HfB_2–30 vol % SiC UHTC samples obtained at various temperatures

Production temperature, °C	ρ, g/cm^3	ρ_{rel}*, %	Calculated porosity*, %	dl/l_0, %	L, nm	σ, MPa	Δm, %
1600	5.35 ± 0.50	60.8 ± 5.7	39.2 ± 5.7	51.2 ± 4.0	48 ± 3	164	0.43
1700	7.55 ± 0.08	85.8 ± 1.0	14.2 ± 1.0	67.7 ± 0.6	37 ± 2	284	0.20
1800	7.86 ± 0.20	89.2 ± 2.3	10.7 ± 2.3	68.9 ± 0.7	36 ± 2	538	0.14
1900	7.83 ± 0.15	89.0 ± 1.7	11.0 ± 1.7	68.1 ± 0.5	38 ± 4	>555	0.17

* Determined in comparison with the calculated density values obtained by additive scheme (the HfB_2 and SiC densities were taken to be 11.2 g/cm^3 [66] and 3.2 g/cm^3 [67]).

to be related to the existing temperature gradient in the bulk of the material, which leads to the incompleteness of the carbothermal SiC synthesis. This conclusion was also confirmed by the X-ray powder diffraction data (Fig. 5). For example, for the products obtained at the hot pressing temperature 1600°C, the X-ray powder diffraction patterns of all the UHTC samples have an intense diffuse halo characterizing the unreacted silicon dioxide in HfB_2–(SiO_2–C) composite powder.

Calculated by the Scherrer formula, the average size of silicon carbide crystallites for the materials synthesized under the mildest conditions (for which the carbothermal synthesis was incomplete) is 48 ± 3 nm, and for the products obtained at the higher temperatures (1700–1900°C), this size is within the range 35–38 nm.

The scanning electron microscopy showed that, for the HfB_2–30 vol % SiC UHTC samples produced at 1600°C, the central and peripheral parts differ not only in color but also in microstructure (cleaved samples, Fig. 6). In the edge zones, in which the conversion in the carbothermal synthesis is higher, the microstructure is less porous than that in the central part, the components are quite uniformly distributed in each other, the HfB_2 grain size is close to that in the initial powders and varies within the range 1–2 μm, and the SiC agglomerate size varies over a much wider range from 100 nm to ~1 μm. At the same time, the phase-contrast imaging showed that, at the center of the samples, there is a large amount of the third component—carbon from the unreacted initial system SiO_2–C. Both the carbon-containing system and the silicon carbide formed from it have lamellar morphology.

At the hot pressing temperatures 1700–1900°C, much denser ceramics form, in which the components are distributed uniformly enough (as also confirmed by mapping, Fig. 7) and the SiC grain size is smaller—to 500–600 nm.

The values of the compressive strength σ (Table 1) also indicate that, with increasing temperature of hot pressing of HfB_2–(SiO_2–C) composite powder, the ceramic being produced is systematically compacted. The strength of the material obtained at 1800°C is close to the instrument determination limit ~538 MPa (which is almost twice as high as the value for sample produced at 1700°C), and at 1900°C, σ exceeds 555 MPa.

To study the thermal behavior of the obtained materials, specimens of equal volume—cylinders ~3 mm in diameter and ~1 mm in height—were cut from samples. Note that the DSC specimens were not identical in shape; therefore, the obtained data suggested only trends in the UHTC oxidation resistance on heating. The experiments were performed in an air flow at a flow rate of 250 mL/min within the temperature range 20–1400°C at a heating rate of 20 deg/min. Figure 8 presents the total DSC and TGA curves for the HfB_2–30 vol % SiC UHTC samples obtained at the temperatures 1600 and 1800°C, and the data on the weight gain by oxidation are summarized in Table 1.

As is seen, the sample obtained at the minimum temperature (1600°C) early in the treatment experiences a weight loss: initially, by desorption, and then, above 400–600°C, by burnout of the unreacted carbon. At 600–800°C, this process is accompanied by the incipient oxidation of the components, first of all, HfB_2, which is indicated by the shape of the exothermic thermal event. Above 800°C, the latter process dominates, which results in a weight gain of 0.43%.

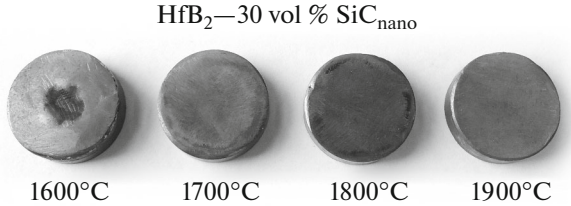

Fig. 4. Appearance of the HfB_2–30 vol % SiC UHTC samples obtained at various temperatures.

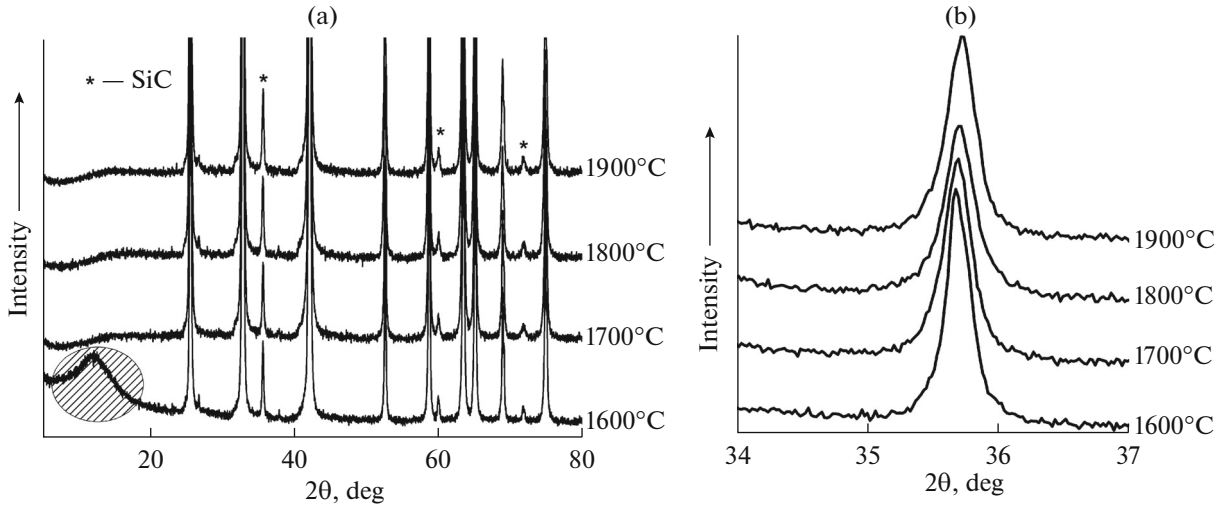

Fig. 5. X-ray powder diffraction patterns of the HfB_2–30 vol % SiC UHTC samples obtained at various temperatures.

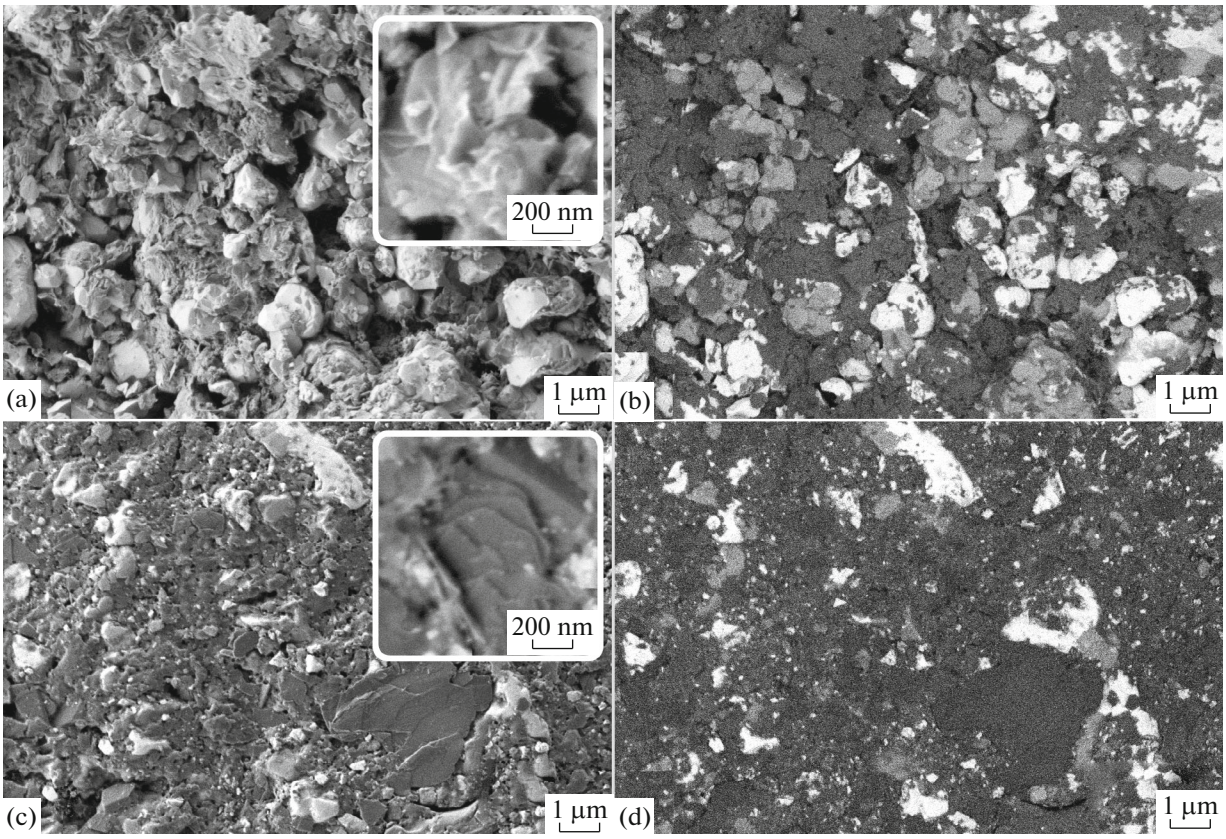

Fig. 6. Microstructure of the cleaved surface of the HfB_2–30 vol % SiC sample obtained at the temperature 1600°C in the (a, b) central and (c, d) peripheral parts of the sample in (a, c) secondary-electron and (b, d) *Z*-contrast images.

However, even for the sample produced at 1700°C, the weight loss due to carbon burnout is lower (0.07%), and at the higher sintering/carbothermy temperatures, there is no such a process (Fig. 8b).

As the data in Table 1 show, at constant composition of the material (30 vol % SiC), the oxidation resistance is strongly affected by the porosity of the obtained samples. For example, for the most porous

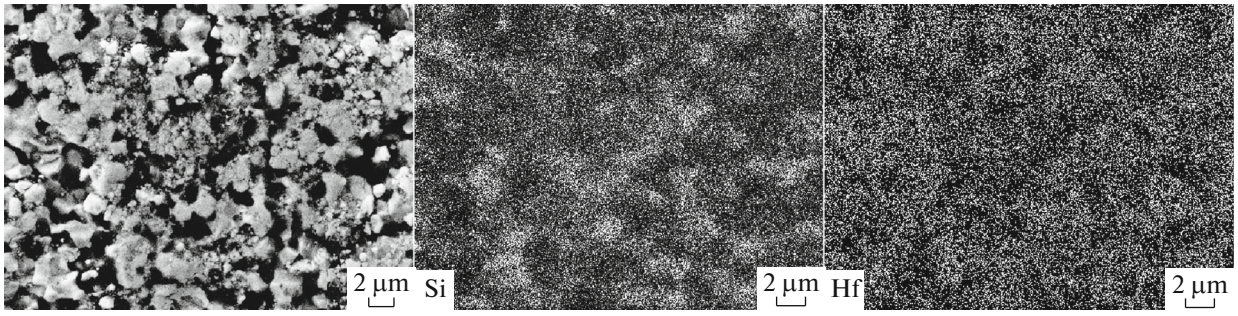

Fig. 7. Microstructure of the cleaved surface of the HfB_2–30 vol % SiC sample obtained at the temperature 1800°C and the silicon and hafnium elemental maps.

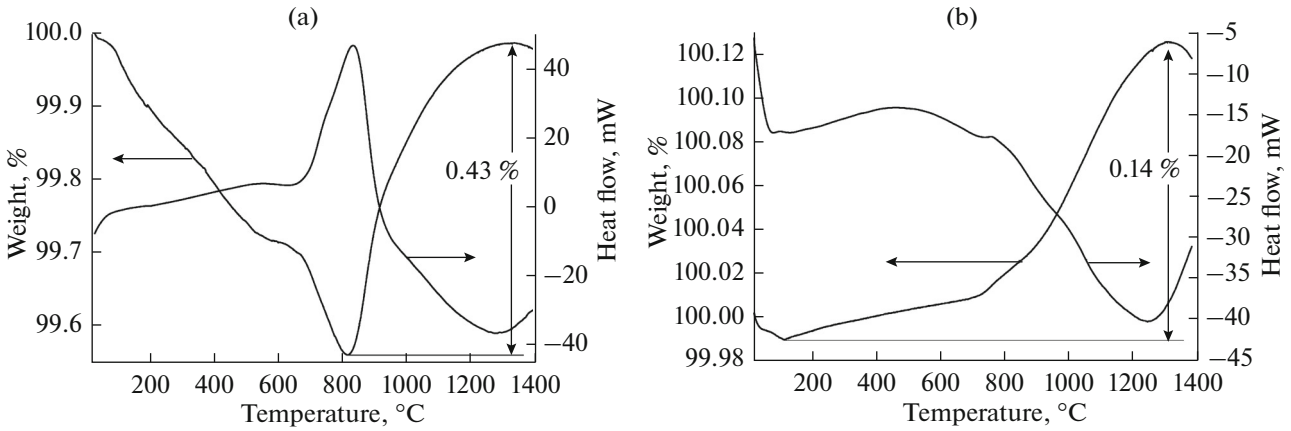

Fig. 8. Thermal behavior in an air flow for the HfB_2–30 vol % SiC samples obtained at the temperatures (a) 1600 and (b) 1800°C.

sample produced at 1600°C, the weight gain is the maximum, which is also influenced by the fact that the carbothermal synthesis is incomplete, and after the burnout of the unreacted carbon, additional porosity forms, favoring oxidation. For the samples obtained at the other temperatures (1700–1900°C), in which the synthesis is completed, the weight gain is the higher, the higher is the porosity of the samples, with the weight gain range being quite narrow (0.14–0.20%). However, although the porosity of one of the samples (hot-pressed at 1600°C) is high (39.2 ± 5.7%), the weight gain of the sample of the given composition (30 vol % SiC) by oxidation does not exceed 0.43%.

Thus, by analyzing the totality of the data on the density of the obtained HfB_2–SiC (30 vol % SiC) UHTCs and the linear shrinkage during hot pressing, the X-ray powder diffraction data, the results of the microstructural analysis, and the thermal behavior in an air flow with aiming at the maximum decrease in the process temperature (to prevent the growth of grains in the ceramics being produced), the optimum synthesis/sintering temperature was chosen to be 1800°C.

Production and Investigation of HfB_2–SiC (10–65 vol % SiC) UHTCs

The preliminary experiments demonstrated that, during hot pressing of HfB_2–$x(SiO_2$–C) composite powders with simultaneous carbothermal synthesis of nanocrystalline SiC at 1800°C, the intense compaction of the initial powders of various compositions begins even on the application of the minimum pressure (5 MPa) at relatively low temperatures (900–1000°C) and significantly accelerates at ≥1600°C. After reaching the required values of pressure (30 MPa) and temperature (after treatment for 15 min), there is additional compaction. Generally (Table 2), with increasing the concentration of the fine SiO_2–C component in the initial HfB_2–$x(SiO_2$–C) powders, the linear shrinkage increases (except for a small deviation for the composition HfB_2–35 vol % SiC). This is consistent with notion that the carbothermal synthesis of SiC gives rise to additional pores, which can collapse during the compaction of the emerging HfB_2–SiC_{nano} system.

This is also evidenced by the change in the density and in the calculated porosity of the produced ceramic materials (Table 2, Fig. 9). As is seen, for a number of

Table 2. Density ρ, calculated porosity, linear shrinkage dl/l_0 during hot pressing, compressive strength σ, and average crystallite size L for the HfB_2–xSiC (x = 10–65 vol %) UHTC samples obtained at the temperature 1800°C

x, vol % SiC	ρ, g/cm^3	ρ_{rel}*, %	Calculated porosity*, %	dl/l_0, %	σ, MPa	L, nm
10	8.69 ± 0.08	83.6 ± 0.8	16.4 ± 0.8	52.3 ± 0.5	>555	42 ± 3
15	8.42 ± 0.04	84.2 ± 0.4	15.8 ± 0.4	61.9 ± 0.3	>555	41 ± 3
20	8.54 ± 0.18	88.9 ± 1.9	11.1 ± 1.9	67.7 ± 3.3	>555	38 ± 2
25	8.21 ± 0.20	89.2 ± 2.2	10.8 ± 2.2	69.4 ± 0.4	519	38 ± 1
30	7.86 ± 0.20	89.3 ± 2.3	10.7 ± 2.3	68.9 ± 0.7	538	36 ± 2
35	6.81 ± 0.15	81.1 ± 1.7	18.9 ± 1.7	65.5 ± 1.6	>555	41 ± 2
45	5.85 ± 0.16	77.0 ± 2.2	23.0 ± 2.2	76.0 ± 1.0	>555	51 ± 1
55	4.64 ± 0.19	68.3 ± 2.9	31.7 ± 2.9	73.4 ± 1.9	>555	55 ± 3
65	3.78 ± 0.13	63.0 ± 2.1	37.0 ± 2.1	75.3 ± 1.1	206	60 ± 2

*Determined in comparison with the calculated density values obtained by additive scheme (the HfB_2 and SiC densities were taken to be 11.2 g/cm^3 [66] and 3.2 g/cm^3 [67]).

compositions—from 20 to 30 vol %, the porosity reaches the minimum and is, on the average, ~11%, and for compositions at higher silicon carbide contents (≥35 vol % SiC), the porosity monotonically increases to ~37%.

Figure 10 presents the appearance of typical obtained samples. All of them are generally dense samples of gray color with metallic luster on the cleaved surface. It was determined that, with increasing silicon carbide content of the produced HfB_2–SiC (≥35 vol % SiC) UHTCs, the porosity of the materials noticeably increases, and there are inclusions of the excess carbon remaining after the carbothermal synthesis (because in the initial powders the ratio n(C) : $n(SiO_2)$ = 1 : 3.05 is established). These inclusions should not worsen the oxidation resistance of the samples: there is evidence of successful testing of samples with intentionally introduced strengthening carbon components (graphite, carbon black, carbon fibers, nanotubes, and graphene).

The X-ray powder diffraction data confirmed that the chosen conditions of hot pressing (temperature 1800°C, heating rate 10 deg/min, treatment time 15 min, pressure 30 MPa, argon medium) of the samples of all the compositions make it possible to perform the complete conversion of silicon dioxide to silicon carbide (Fig. 11). This was also corroborated by the reflection IR spectroscopy data. Calculated by the Scherrer formula, the average size of SiC crystallites in all the systems are within the range 36–60 nm. In three least porous samples containing 20, 25, and 30 vol % SiC, the coherent scattering domain sizes are the minimum: 36–38 nm. At the same time, in the samples containing ≥35 vol % SiC, with increasing their porosity, the average crystallite size increases significantly: from ~41 nm at 35 vol % SiC to ~60 nm at 65 vol % SiC.

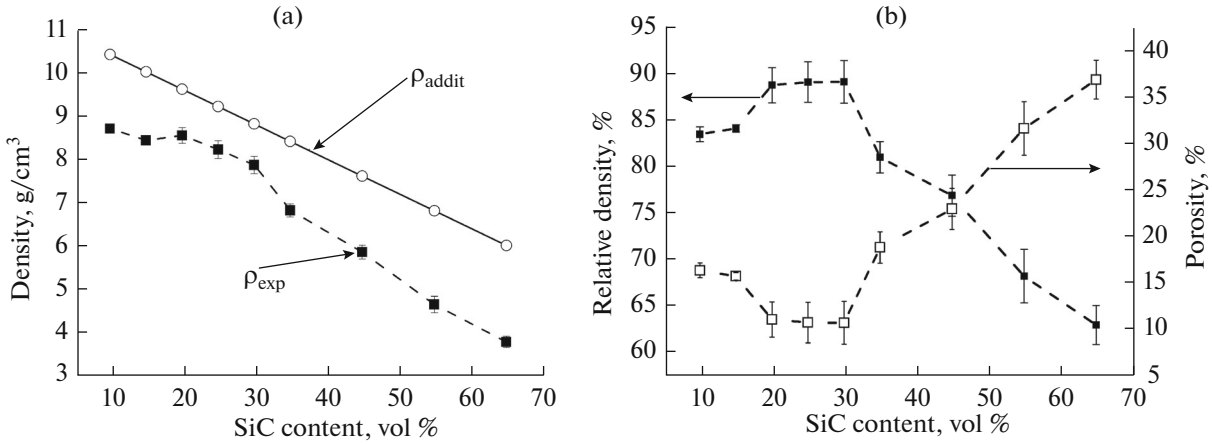

Fig. 9. (a) Experimental and calculated (by additive scheme) densities and (b) the relative density and porosity of the obtained HfB_2–xSiC (x = 10–65 vol %) samples.

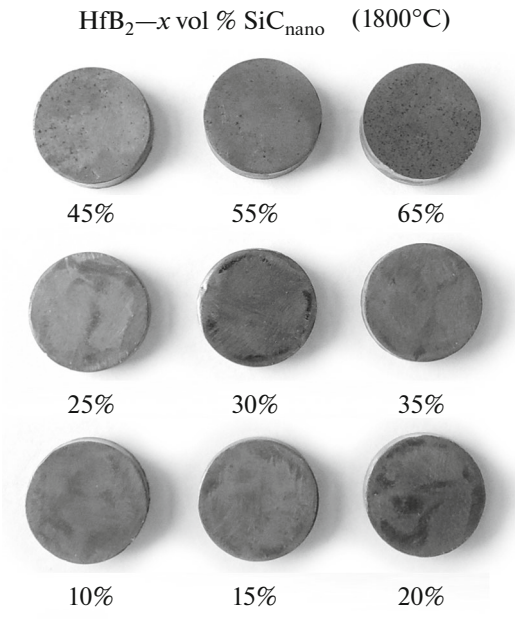

Fig. 10. Appearance of the HfB_2–xSiC (x = 10–65 vol %) UHTC samples obtained by hot pressing of HfB_2–$x(SiO_2$–C) composite powders.

It should be separately noted that, in all the obtained samples, regardless of the HfB_2 : SiC ratio and the porosity, there is no impurity phase HfO_2, which can form by the interaction of the initial HfB_2 powder with SiO_2, SiO, or carbon oxides, and also there is no hafnium carbide phase, which suggests that the chosen conditions of hot pressing/synthesis favors the necessary reaction between the fine components of the SiO_2–C composite synthesized by the sol–gel method.

The microstructure of the cleaved surfaces of the obtained samples does not differ fundamentally from that for the above HfB_2–30 vol % SiC UHTC samples produced at the temperature 1800°C: the synthesized SiC is localized between HfB_2 particles to form aggregates 200–1000 nm in diameter (Fig. 12).

The determination of the compressive strength σ gave values of >500 MPa for almost all of the samples, with the exception of the sample with the maximum fine silicon carbide content and the highest porosity, for which a much lower strength value found (206 MPa).

To investigate the thermal behavior of the obtained materials, specimens were produced similar to those (cylinders of equal volume) used for studying the HfB_2–30 vol % SiC UHTC samples. As an example, Fig. 13 presents the results for the samples containing 10, 20, 35, and 65 vol % SiC, and the data on the weight gain by oxidation were summarized in Table 3 and Fig. 14. As Fig. 13 shows, at the minimum silicon carbide content (10 vol %) and a porosity of 16%, even at the temperature 1400°C, there is a trend toward a further weight gain by oxidation, which may suggest that such an amount of SiC is insufficient to form a protective borosilicate glass layer. At a content of as low as 15 vol % SiC, at a temperature of ~1330°C, Δm plateaus and halves: from 0.50% at 10 vol % SiC to 0.27% at 15 vol % SiC. With a further increase in the silicon carbide content (to 20 vol %) and an abrupt decrease in the porosity to ~11%, Δm does not radically change (Δm = 0.20%).

For the HfB_2–x vol % SiC (x = 25–30) UHTC samples at the minimum porosity ~11%, the weight

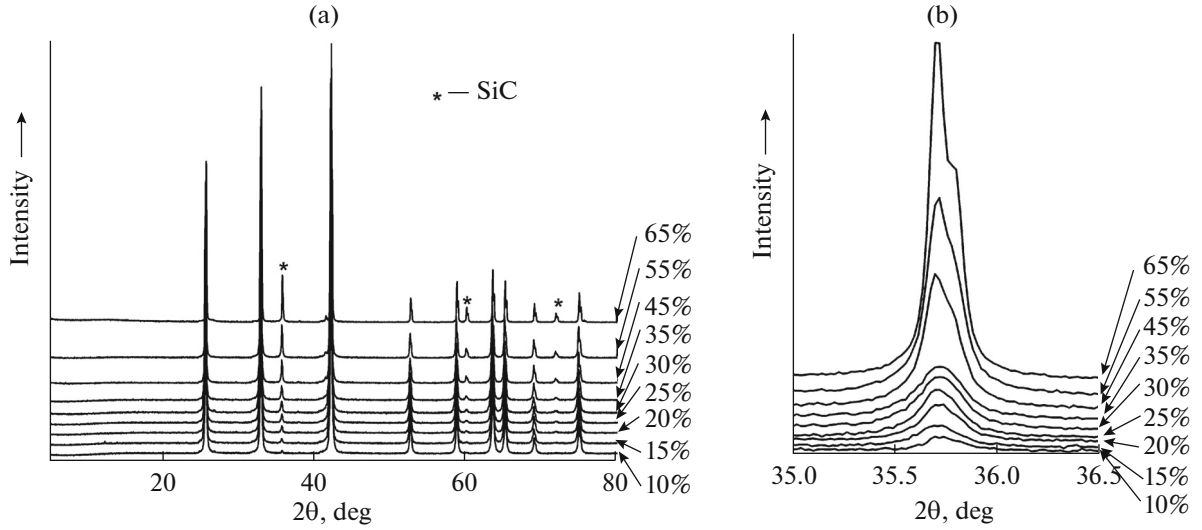

Fig. 11. X-ray powder diffraction patterns of the HfB_2–xSiC (x = 10–65 vol %) UHTC samples obtained by hot pressing of HfB_2–$x(SiO_2$–C) composite powders.

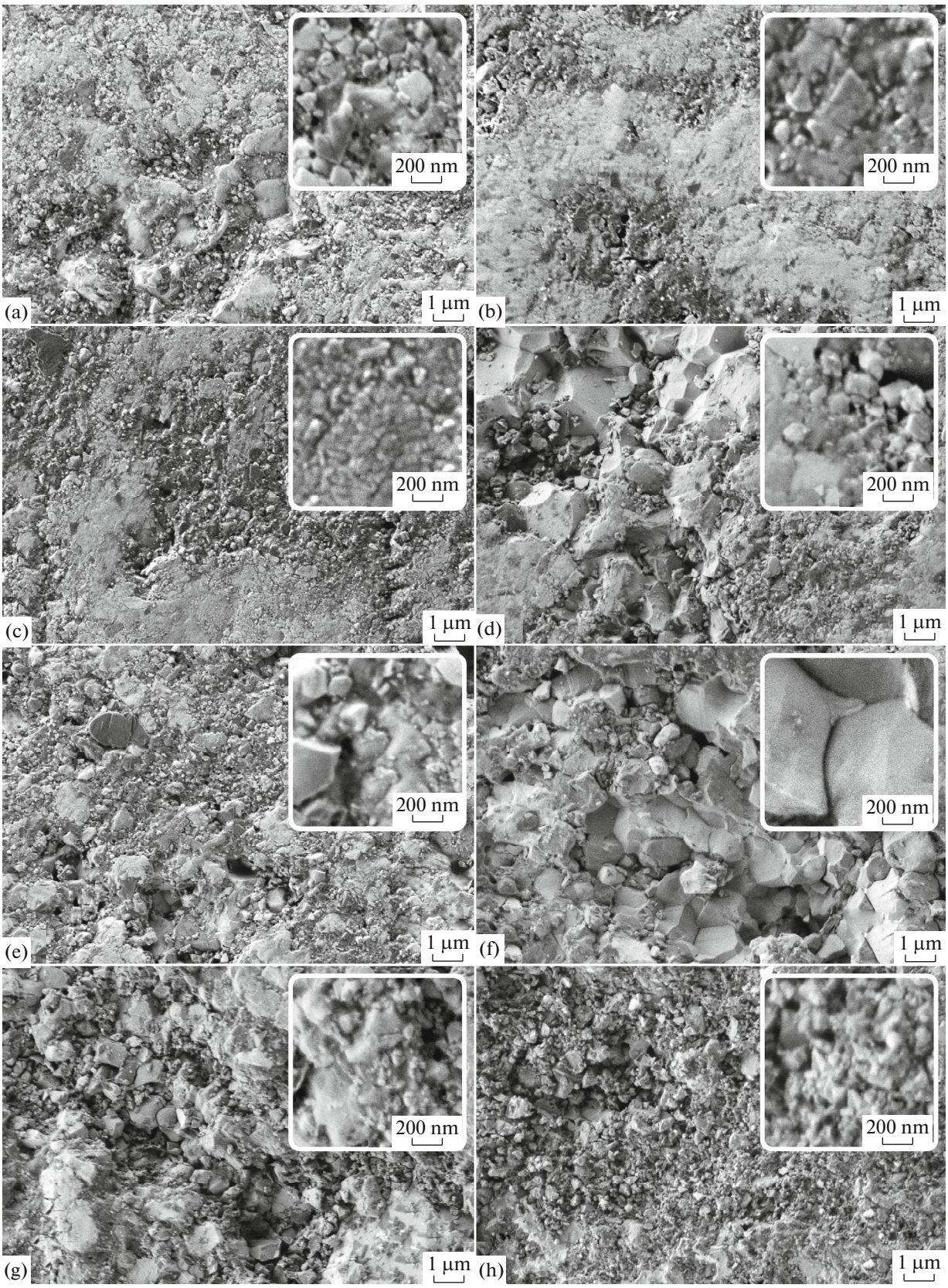

Fig. 12. Microstructure of the cleaved surfaces of the HfB_2–x vol % SiC samples obtained at the temperature 1800°C at x = (a) 10, (b) 15, (c) 20, (d) 25, (e) 35, (f) 45, (g) 55, and (h) 65.

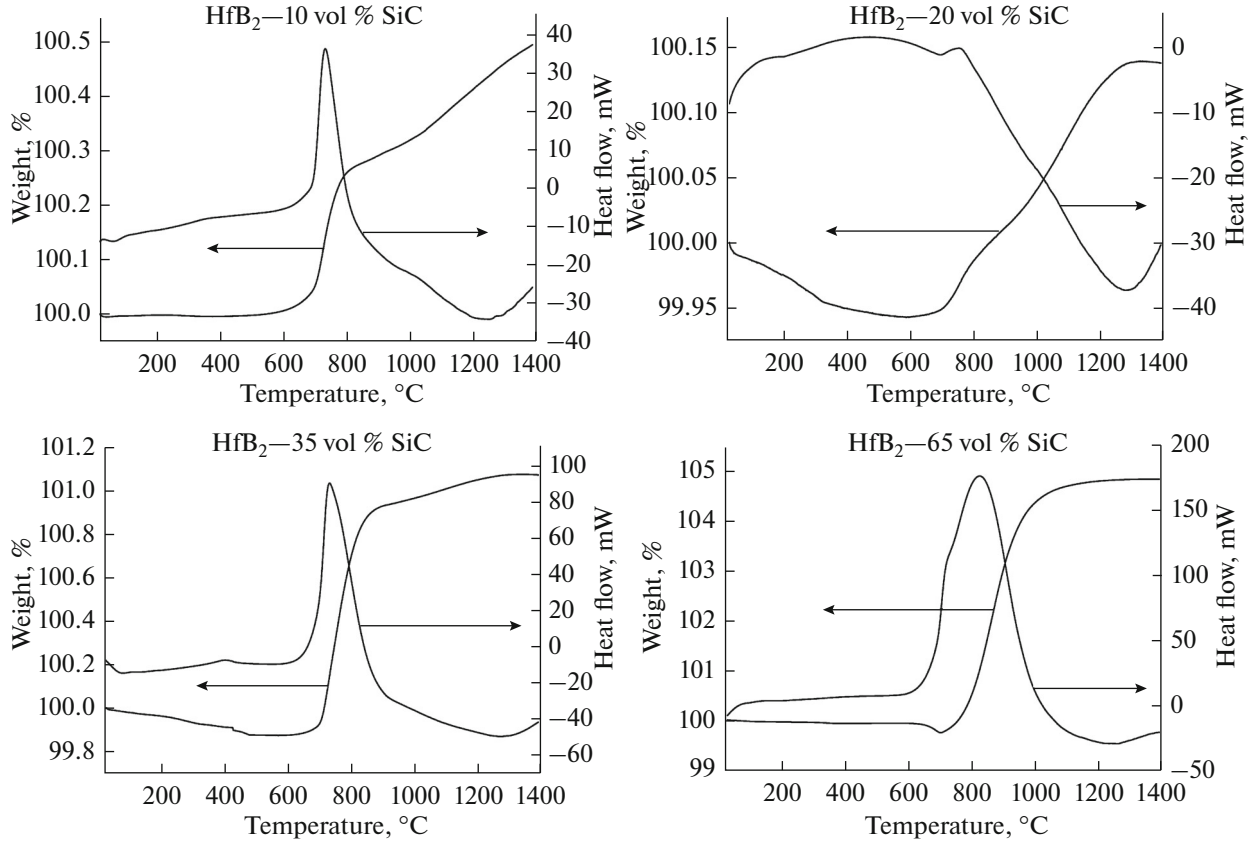

Fig. 13. DSC and TGA curves for the HfB_2–x vol % SiC samples obtained at the temperature 1800°C at x = 10, 20, 35, and 65.

gain is 0.14–0.18%; however, the TGA curves at temperatures above 800°C do not plateau but have a broadened maximum of low intensity. Probably, at such insignificant weight gains, the weight loss due to B_2O_3 evaporation at temperatures >1200–1300°C becomes significant.

An increase in the SiC content to 35 vol % leads to an increase in the porosity to ~19%, and the weight gain is 1.20%. The TGA curves have two-step plateaus (as for the sample containing 45 vol % SiC): the first step at 870–900°C and the second step at 1190–1240°C.

For the HfB_2–x vol % SiC (x = 55–65) UHTC samples with similar and high porosities (32–37%), the weight gain is much higher (to 5–6%), the oxidation starts at higher temperature, and the sample weight has a one-step plateau at lower temperature (1070–1125°C). This may be due to the presence of a large amount of nanodispersed and, hence, reactive silicon carbide, which usually begins to be oxidized at temperatures above 750–800°C. Besides, these samples are characterized by a low (0.1–0.2%) weight loss at ~650–720°C due to the burnout of a part of the excessively introduced carbon, which may lead to a certain error in calculating the weight gain due to the oxidation of the samples because the processes of the oxidation of carbon (accompanied by weight loss) and HfB_2 and SiC (accompanied by weight gain) occur virtually simultaneously.

Figure 14 summarizes the data on the weight gain for all the samples. As is seen, the samples can be con-

Table 3. Weight gain Δm due to oxidation in an air flow during heating to the temperature 1400°C for the HfB_2–xSiC (x = 10–65 vol %) UHTC samples obtained at the temperature 1800°C, approximate temperature $T_{m=\text{const}}$ at which the weight gain plateaus, and porosity of the samples

SiC content, vol %	Δm, %	$T_{m=\text{const}}$, °C	Calculated porosity, %
10	0.50	–	16.4 ± 0.8
15	0.27	1330	15.8 ± 0.4
20	0.20	1280	11.1 ± 1.9
25	0.18	1315*	10.8 ± 2.2
30	0.14	1315*	10.7 ± 2.3
35	1.20	875/1240	18.9 ± 1.7
45	1.27	900/1190	23.0 ± 2.2
55	6.26	1125	31.7 ± 2.9
65	5.07	1070	37.0 ± 2.1

*Temperature of the maximum in the weight curve.

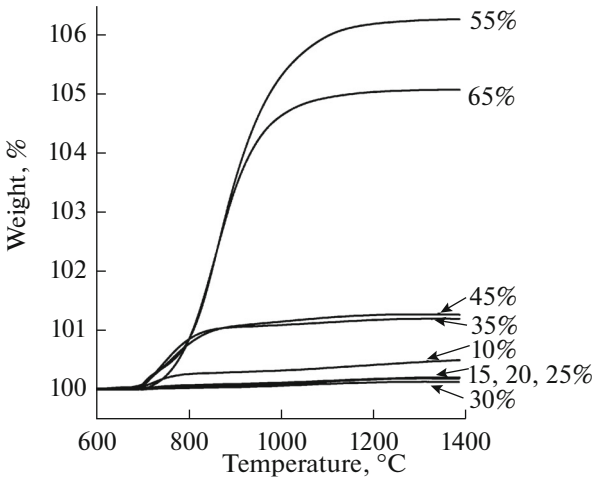

Fig. 14. TGA curves for the HfB_2–*x* vol % SiC (*x* = 10–65) samples obtained at the temperature 1800°C.

ditionally divided into several groups. The first group contains the samples with the maximum SiC content (55 and 65 vol %), the maximum porosity, and the maximum weight gain due to oxidation. The second group comprises the HfB_2–*x* vol % SiC (*x* = 35–45) samples, which, despite significant differences in composition and porosity (19% at *x* = 35 vol % SiC and 23% at *x* = 45 vol % SiC), have very close Δm values (1.2–1.3%). The third group is constituted by the samples with the minimum (0.14–0.27%) weight gain and the SiC content 15–30 vol % at a porosity of 11–16%. Somewhat apart is the HfB_2–10 vol % SiC sample, for which the weight gain due to oxidation is also low: 0.50% at a porosity of 16.4%.

The obtained data suggest that the oxidation resistance of the produced composites at temperatures to 1400°C is significantly influenced both by the composition, and the porosity, i.e., the microstructure.

The X-ray powder diffraction analysis of the surface of the samples after their oxidation under identical conditions showed that the phase composition is significantly dependent on the composition of the initial material (Fig. 15). For the samples containing 10–20 vol % SiC, there are reflections of monoclinic HfO_2 and the HfB_2 phase (the unoxidized layers of the material probably manifest themselves). For the HfB_2–25 vol % SiC sample, on the surface, a hafnon $HfSiO_4$ phase emerges (~23%), the concentration of which decreases to ~2–5% with increasing silicon carbide content of UHTC. Beginning with the HfB_2–35 vol % SiC sample, in the X-ray powder diffraction patterns, reflections of the silicon carbide phase emerge, the concentration of which increases with decreasing concentration of the HfB_2 phase, thus representing changes in the composition of the initial materials. In general, the content of the crystalline oxidation products (both $HfSiO_4$, and HfO_2) decreases with increasing SiC content of the HfB_2–*x* vol % SiC samples, which may suggest that protective X-ray amorphous borosilicate glass is primarily localized on the surface.

To compare the oxidation resistances of the materials obtained by our proposed method based on the carbothermal synthesis occurring directly during hot pressing of HfB_2–(SiO_2–C) composite powders

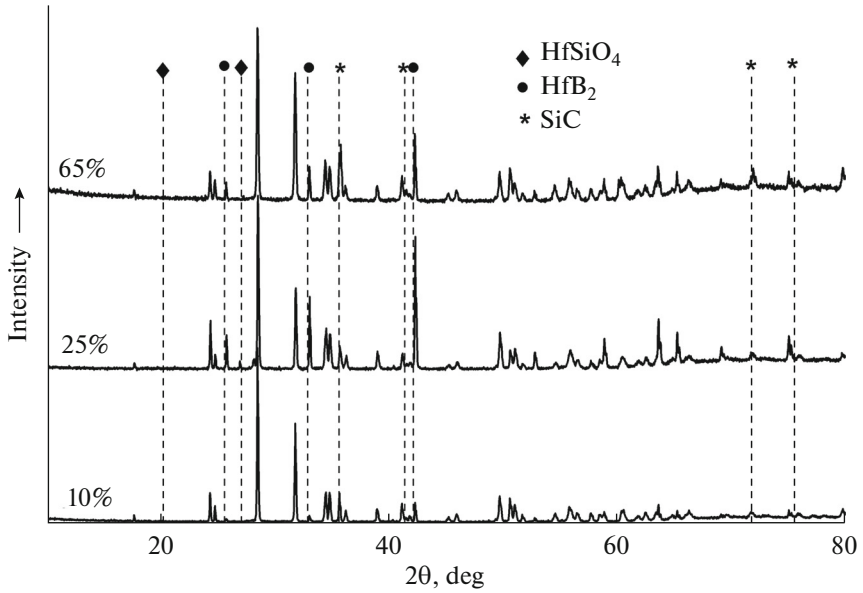

Fig. 15. X-ray powder diffraction patterns of the surface of the HfB_2–*x*SiC (*x* = 10, 25, and 65 vol %) samples after their oxidation in an air flow under the DCS/TGA conditions. The unlabeled reflections represent the monoclinic HfO_2 phase.

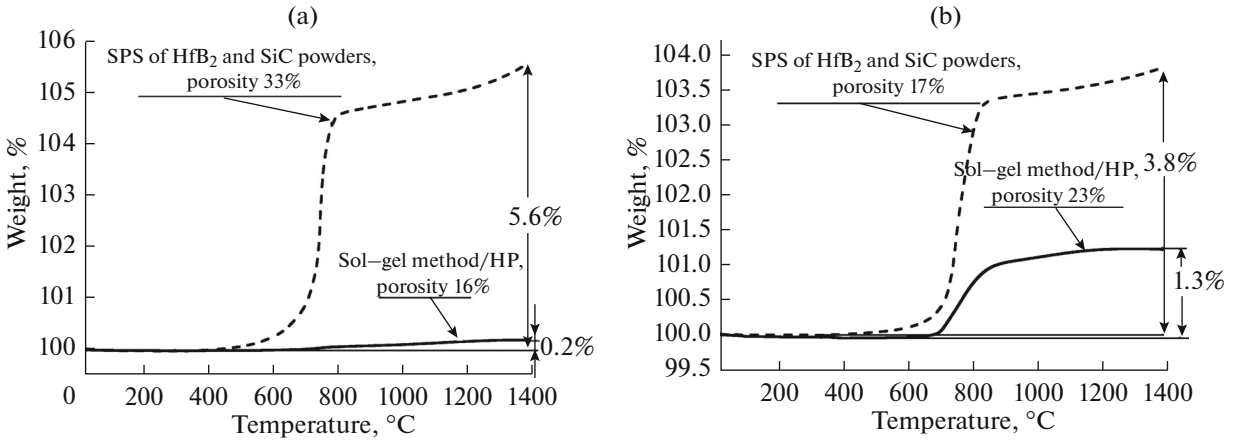

Fig. 16. TGA curves for the HfB_2–*x* vol % SiC samples at *x* = (a) 15 and (b) 45 that were obtained by spark plasma sintering (SPS) of coarse HfB_2 and SiC powders (dashed lines) and by our proposed method based on hot pressing (HP) of HfB_2–(SiO_2–C) composite powders (solid lines).

obtained by the sol–gel method and UHTC produced by spark plasma sintering from commercially available powders HfB_2 and SiC, we performed the thermal analysis in an air flow for samples of identical composition (HfB_2–15 vol % SiC) (Fig. 16a, specimens of similar shapes, similar experimental conditions).

It was found that, for a sample obtained by spark plasma sintering of HfB_2 and SiC powders, the weight gain due to oxidation was 5.62%, whereas for a sample of the same composition that was produced by the sol–gel method combined with hot pressing of HfB_2–(SiO_2–C) composites, Δm is 0.21%. Such a great difference in oxidation resistance (by a factor of 27) could be explained only by much larger porosity of the former sample (33% as compared to 16%); therefore, we additionally studied the oxidation resistance of samples that had identical compositions and similar porosities but were obtained by different methods.

The additional experiments for investigating the oxidation resistance of samples of the composition HfB_2–45 vol % SiC for which the porosity ratio was inverse (the porosity of the sample obtained by spark plasma sintering from HfB_2 and SiC powders was 17%, and the porosity of the hot-pressed HfB_2–(SiO_2–C) composite powder was 23%; i.e., the weight gain could be expected to be higher for the latter sample) demonstrated that, in this case, too, Δm due to the oxidation of the material for the latter sample is thrice as low (Fig. 16b) as that for the sample of the same composition that was produced by spark plasma sintering of powders.

The obtained data showed that, owing to microstructural features, namely, the protection of the surface of HfB_2 particles by nanocrystalline silicon carbide, highly reactive in reactions with oxygen, the proposed method offers additional opportunities for increasing the oxidation resistance in comparison with conventional methods thanks to the formation of a protective borosilicate glass layer at lower temperatures.

Thus, it was demonstrated that the chosen conditions of hot pressing/carbothermal synthesis (temperature 1800°C, treatment time 15 min, pressure 30 MPa) make it possible to produce, based on HfB_2–(SiO_2–C) composite powders obtained by the sol–gel method, more oxidation-resistant HfB_2–*x* vol % SiC (*x* = 10–65) UHTCs. It was shown that the oxidation resistance of the obtained materials is significantly dependent both on their density, and on their composition.

CONCLUSION

In this work, a new method was proposed for producing ultra-high-temperature ceramics MB_2–SiC, where M = Zr, Hf. The method differs in the fact that, owing to the high reactivity of the SiO_2–C system synthesized on the surface of metal diboride particles by the sol–gel method, the hot pressing of intermediate product HfB_2–(SiO_2–C) under relatively mild conditions (30 MPa, 1700–1900°C) not only produces a ceramic with comparatively high compressive strength (≥500 MPa), but also leads to the synthesis of one of the components (SiC) in the nanosized state (average crystallite size 36–61 nm). This reduces energy consumption not only owing to the decrease in the hot pressing temperature, but also thanks to the elimination of a separate stage of high-temperature synthesis of nanocrystalline SiC powder and subsequent stages of mixing and mutual grinding of HfB_2 and the obtained SiC powder.

It was experimentally established that the oxidation resistance of the produced HfB_2–SiC (10–65 vol % SiC) UHTCs during heating in an air flow to 1400°C under the TGA/DCS conditions exceeds that of the materials of the same composition that were obtained

by spark plasma sintering of coarse HfB_2 and SiC powders, even if the density of these powders is higher. This is likely to be due to the fact that, because of the high reactivity of nanocrystalline silicon carbide, a protective borosilicate glass layer forms at lower temperatures.

ACKNOWLEDGMENTS

This work was supported by the Russian Science Foundation (project no. 17-73-20181).

REFERENCES

1. E. P. Simonenko, D. V. Sevast'yanov, N. P. Simonenko, et al., Russ. J. Inorg. Chem. **58**, 1669 (2013). doi 10.1134/S0036023613140039
2. L. Silvestroni, H.-J. Kleebe, W. G. Fahrenholtz, and J. Watts, Sci. Rep. **7**, Art. no. 40730 (2017). doi 10.1038/srep40730
3. E. P. Simonenko, A. N. Gordeev, N. P. Simonenko, et al., Russ. J. Inorg. Chem. **61**, 1203 (2016). doi 10.1134/S003602361610017X
4. M. Mallik, A. J. Kailath, K. K. Ray, et al., J. Eur. Ceram. Soc. **37**, 559 (2017). doi 10.1016/j.jeurceramsoc.2016.09.024
5. A. Nisar, S. Ariharan, T. Venkateswaran, et al., Carbon **111**, 269 (2017). doi 10.1016/j.carbon.2016.10.002
6. V. G. Sevast'yanov, E. P. Simonenko, A. N. Gordeev, et al., Russ. J. Inorg. Chem. **58**, 1269 (2013). doi 10.1134/S003602361311017X
7. M. Asl Shahedi, F. Golmohammadi, M. Ghassemi Kakroudi, and M. Shokouhimehr, Ceram. Int. **42**, 4498 (2016). doi 10.1016/j.ceramint.2015.11.139
8. M. Asl Shahedi, M. Ghassemi Kakroudi, I. Farahbakhsh, et al., Ceram. Int. **42**, 18612 (2016). doi 10.1016/j.ceramint.2016.08.20
9. V. G. Sevastyanov, E. P. Simonenko, A. N. Gordeev, et al., Russ. J. Inorg. Chem. **59**, 1298 (2014). doi 10.1134/S0036023614110217
10. V. G. Sevastyanov, E. P. Simonenko, A. N. Gordeev, et al., Russ. J. Inorg. Chem. **59**, 1361 (2014). doi 10.1134/S0036023614120250
11. L. Wang, D. Kong, G. Fang, and J. Liang, Int. J. Appl. Ceram. Technol. **14**, 31 (2017). doi 10.1111/ijac.12613
12. V. G. Sevastyanov, E. P. Simonenko, A. N. Gordeev, et al., Russ. J. Inorg. Chem. **60**, 1360 (2015). doi 10.1134/S0036023615110133
13. M. Patel, V. Singh, and V. V. B. Prasad, Oxid. Met. **86**, 339 (2016).
14. D. V. Grashchenkov, O. Yu. Sorokin, Yu. E. Lebedeva, and M. L. Vaganova, Russ. J. Appl. Chem. **88**, 386 (2015).
15. Yu. B. Lyamin, V. Z. Poilov, E. N. Pryamilova, et al., Russ. J. Inorg. Chem. **61**, 149 (2016). doi 10.1134/S0036023616020133
16. W. Tan, M. Adducci, C. Petorak, et al., J. Eur. Ceram. Soc. **36**, 3833 (2016). doi 10.1016/j.jeurceramsoc.2016.04.013
17. D. L. Poerschke, M. D. Novak, N. Abdul-Jabbar, et al., J. Eur. Ceram. Soc. **36**, 3697 (2016). doi 10.1016/j.jeurceramsoc.2016.05.048
18. D. V. Kolovertnov and I. B. Ban'kovskaya, Glass Phys. Chem. **41**, 324 (2015).
19. B. Du, N. Li, B. Ke, et al., Ceram. Int. **42**, 14292 (2016). doi 10.1016/j.ceramint.2016.06.041
20. Y. An, X. Xu, and K. Gui, Ceram. Int. **42**, 14066 (2016). doi 10.1016/j.ceramint.2016.06.014
21. X. Jin, L. Dong, Q. Li, et al., Ceram. Int. **42**, 13309 (2016). doi 10.1016/j.ceramint.2016.05.040
22. B. Zhang, X. Zhang, C. Hong, et al., ACS Appl. Mater. Interfaces **8**, 11675 (2016). doi 10.1021/acsami.6b00822
23. H. Jin, S. Meng, X. Zhang, et al., J. Am. Ceram. Soc. **99**, 2474 (2016). doi 10.1111/jace.14232
24. L. A. Chevykalova, I. Yu. Kelina, I. L. Mikhal'chik, et al., Refract. Ind. Ceram. **54**, 455 (2014).
25. X. Jin, L. Dong, H. Xu, et al., Ceram. Int. **42**, 9051 (2016). doi 10.1016/j.ceramint.2016.02.164
26. H. Jin, S. Meng, X. Zhang, et al., J. Eur. Ceram. Soc. **36**, 1855 (2016). doi 10.1016/j.jeurceramsoc.2016.02.040
27. Yoon D.-H. Muksin and K. Raju, Ceram. Int. **42**, 7300 (2016). doi 10.1016/j.ceramint.2016.01.126
28. Y. Yuan, J.-X. Liu, and G.-J. Zhang, Ceram. Int. **42**, 7861 (2016). doi 10.1016/j.ceramint.2016.01.067
29. Z. Kovacova, L. Baca, E. Neubauer, and M. Kitzmantel, J. Eur. Ceram. Soc. **36**, 3041 (2016). doi 10.1016/j.jeurceramsoc.2015.12.028
30. H. Jin, S. Meng, X. Zhang, et al., Ceram. Int. **42**, 6480 (2016). doi 10.1016/j.ceramint.2015.12.132
31. M. Asl Shahedi, A. Sabahi Namini, and M. Ghassemi Kakroudi, Ceram. Int. **42**, 5375 (2016). doi 10.1016/j.ceramint.2015.12.072
32. X. Zhang, Z. Chen, X. Xiong, et al., Ceram. Int. **42**, 2798 (2016). doi 10.1016/j.ceramint.2015.11.012
33. Y. Yan, Z. Huang, S. Dong, and D. Jiang, J. Am. Ceram. Soc. **89**, 3589 (2006). doi 10.1111/j.1551-2916.2006.01270.x
34. S. Guo, J. Yang, H. Tanaka, and Y. Kagawa, Compos. Sci. Technol. **68**, 3033 (2008).
35. H. Zhang, Y. Yan, Z. Huang, et al., Key Eng. Mater. **434–435**, 193 (2010). doi 10.4028/www.scientific.net/KEM.434-435.193
36. M. Ikegami, S. Guo, and Y. Kagawa, Ceram. Int. **38**, 769 (2012).
37. V. Zamora, A. L. Ortiz, F. Guiberteau, and M. Nygren, J. Eur. Ceram. Soc. **32**, 2529 (2012).
38. W. Han, S. Zhou, and J. Zhang, Ceram. Int. **40**, 16665 (2014).
39. M. Mashhadi, H. Khaksari, and S. Safi, J. Mater. Res. Technol. **4**, 416 (2015).
40. M. Jaberi Zamharir, M. Shahedi Asl, M. Ghassemi Kakroudi, et al., Ceram. Int. **41**, 9628 (2015).
41. E. P. Simonenko, N. P. Simonenko, G. P. Kopitsa, et al., Russ. J. Inorg. Chem. **61**, 1347 (2016). doi 10.1134/S0036023616110206
42. V. G. Sevastyanov, E. P. Simonenko, N. P. Simonenko, et al., Kompoz. Nanostrukt. **6** (4), 198 (2014).

43. E. P. Simonenko, N. P. Simonenko, A. V. Derbenev, et al., Russ. J. Inorg. Chem. **58**, 1143 (2013). doi 10.1134/S0036023613100215
44. E. P. Simonenko, N. P. Simonenko, V. G. Sevastyanov, and N. T. Kuznetsov, Russ. J. Inorg. Chem. **61**, 1483 (2016). doi 10.1134/S0036023616120172
45. E. P. Simonenko, N. P. Simonenko, D. V. Sevastyanov, et al., Russ. J. Inorg. Chem. **61**, 1649 (2016). doi 10.1134/S0036023616130039
46. H. Zhang, F. Fu, Y. Cao, et al., Interceram. **62**, 282 (2013).
47. T. Wang, Y. Zhang, J. Li, et al., J. Nanosci. Nanotechnol. **15**, 7402 (2015). doi 10.1166/jnn.2015.10583
48. Y. Cao, H. Zhang, F. Li, et al., Ceram. Int. **41**, 7823 (2015). doi 10.1016/j.ceramint.2015.02.117
49. Y. Zhang, Y. Zhang, R.-X. Li, et al., J. Taiwan Inst. Chem. Eng. **46**, 200 (2015). doi 10.1016/j.jtice.2014.09.022
50. B. Zhao, Y. Zhang, J. Li, et al., J. Solid State Chem. **207**, 1 (2013). doi 10.1016/j.jssc.2013.08.028
51. Y. Yan, H. Zhang, Z. Huang, et al., J. Am. Ceram. Soc. **91**, 1372 (2008). doi 10.1111/j.1551-2916.2008.02296.x
52. N. Patra, D. D. Jayaseelan, and W. E. Lee, Adv. Appl. Ceram. **115**, 36 (2016).
53. X. P. Che, S. Z. Zhu, L. J. Yang, and Q. Xu, Adv. Mater. Res. **105–106**, 213 (2010).
54. X. Deng, S. Du, H. Zhang, et al., Ceram. Int. **41**, 14419 (2015).
55. S. Chakraborty, D. Debnath, A. R. Mallick, et al., Int. J. Refract. Met. Hard Mater. **52**, 176 (2015).
56. D. Debnath, S. Chakraborty, A. R. Mallick, et al., Adv. Appl. Ceram. **114**, 45 (2015).
57. M. Jalaly, M. Tamizifar, M. S. Bafghi, and F. J. Gotor, J. Alloys Compd. **581**, 782 (2013).
58. M. Jalaly, M. S.-S. Bafghi, M. Tamizifar, and F. J. Gotor, Int. J. Appl. Ceram. Technol. **12**, 551 (2015).
59. W.-W. Wu, G.-J. Zhang, Y.-M. Kan, and P.-L. Wang, Mater. Lett. **63**, 1422 (2009).
60. H.-C. Oh, S.-H. Lee, and S.-C. Choi, Int. J. Refract. Met. Hard Mater. **42**, 132 (2014).
61. X. Deng, S. Du, H. Zhang, et al., Ceram. Int. **41**, 14419 (2015).
62. N. T. Kuznetsov, V. G. Sevast'janov, E.P. Simonenko, et al., Patent RU no. 2556599, July 10, 2015.
63. E. P. Simonenko, A. V. Derbenev, N. P. Simonenko, et al., Russ. J. Inorg. Chem. **62**, 863 (2017). doi 10.1134/S0036023617070221
64. V. G. Sevastyanov, Y. S. Ezhov, E. P. Simonenko, and N. T. Kuznetsov, Mater. Sci. Forum **457–460**, 59 (2004). doi 10.4028/www.scientific.net/MSF.457-460.59
65. R. G. Pavelko, V. G. Sevast'yanov, Yu. S. Ezhov, and N. T. Kuznetsov, Inorg. Mater. **43**, 700 (2007). doi 10.1134/S0020168507070059
66. W. Wong-Ng, H. F. McMurdie, B. Paretzkin, et al., Powder Diffr. **2**, 257 (1987).
67. T. Kawamura, Mineral. J. **4**, 333 (1965).

Translated by V. Glyanchenko